Estimating Oceanic Primary Production Using Vertical Irradiance and Chlorophyll Profiles from Ocean Gliders in the North Atlantic

Victoria S. Hemsley,*,[†,‡] Timothy J. Smyth,[§] Adrian P. Martin,[‡] Eleanor Frajka-Williams,[†]
Andrew F. Thompson,[∥] Gillian Damerell,[⊥] and Stuart C. Painter[‡]

[‡]National Oceanography Centre, Waterfront Campus, European Way, Southampton, SO14 3ZH, United Kingdom

[†]Ocean and Earth Science, National Oceanography Centre Southhampton, University of Southampton, SO14 3ZH, United Kingdom

[§]Plymouth Marine Laboratory, Prospect Place, The Hoe, Plymouth, PL1 3DH, United Kingdom

[∥]Environmental Science and Engineering, California Institute of Technology, Pasadena, California 91125, United States

[⊥]School of Environmental Sciences, University of East Anglia, Norwich, NR4 7TJ, United Kingdom

S *Supporting Information*

ABSTRACT: An autonomous underwater vehicle (Seaglider) has been used to estimate marine primary production (PP) using a combination of irradiance and fluorescence vertical profiles. This method provides estimates for depth-resolved and temporally evolving PP on fine spatial scales in the absence of ship-based calibrations. We describe techniques to correct for known issues associated with long autonomous deployments such as sensor calibration drift and fluorescence quenching. Comparisons were made between the Seaglider, stable isotope (^{13}C), and satellite estimates of PP. The Seaglider-based PP estimates were comparable to both satellite estimates and stable isotope measurements.
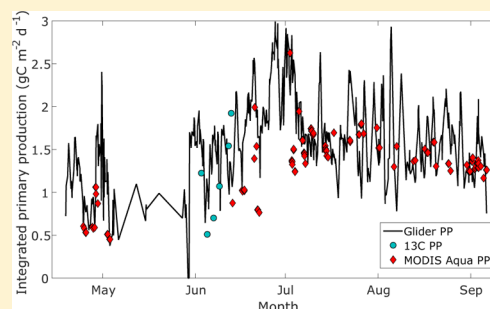
1. INTRODUCTION

Primary production (PP) is the carbon fixed by plants through photosynthesis, the basis of almost all terrestrial and marine food webs. Marine phytoplankton fix 45−50 Gt C yr^{-1}, approximately half of global PP.[1,2] PP is critical for regulating the drawdown of atmospheric carbon dioxide[3] and the air−sea exchange of radiatively important trace gases.[4−6] In situ measurements of PP in the open ocean are sparse and avoid winter, making it difficult to resolve and separate spatial and temporal variability.[1] Regular fixed-point sampling is difficult to extrapolate due to spatial variability. Satellites provide global estimates of oceanic PP over a range of spatial and temporal scales[7−11] but, while satellite-derived surface chlorophyll captures the variability in PP better than any other remotely sensed parameter,[12] it relies on cloud free skies and only observes the top few meters, thereby omitting features such as subsurface chlorophyll maxima (SCM).[13] As a result, PP estimates derived exclusively from satellite data typically underestimate spatial and temporal variability.[1] Methods have been developed to accommodate SCM[14] but are based on broad statistical relationships.[15]

Significant improvements in PP estimates from satellite surface chlorophyll fields are possible with simultaneous in situ chlorophyll and PAR (photosynthetically active radiation) profiles.[12] Underwater gliders provide such data, improving the vertical and temporal resolution of observations.[16,17] However, gliders use fluorescence as proxy for chlorophyll,[19] and long-duration missions may lack sufficient in situ calibration.[18,20]

We describe a method for estimating PP at high vertical and temporal resolution, using glider chlorophyll fluorescence and irradiance profiles. Significantly, it uses irradiance to calibrate fluorescence and, therefore, needs no in situ samples for calibration. This method makes possible depth-resolved continuous estimates of PP over a full seasonal cycle, in all weather.

2. DATA SETS

2.1. Area of Study. Data were collected in the northeast Atlantic Ocean (48°41′ N, 16°11′ W) as part of the OSMOSIS (Ocean Surface Mixing, Ocean Submesoscale Interaction Study). This site is approximately 40 km southeast of the Porcupine Abyssal Plain sustained observatory (Figure 1).[21,22]

Currents in this area are generally weak,[23,24] with mean dive averaged currents of 11 cm s^{-1}. Patchy phytoplankton distributions with fine spatial scales (<10 km) have been observed in this region.[25] Diatoms dominate the spring bloom, succeeded by prymnesiophytes and dinoflagellates.[26,27] In summer, diatoms form an SCM at the base of the mixed layer.[28,29] Due to the patchy nature of the phytoplankton distribution, advection of spatial variability can result in apparent variations in the phytoplankton community structure on daily time scales.[30]
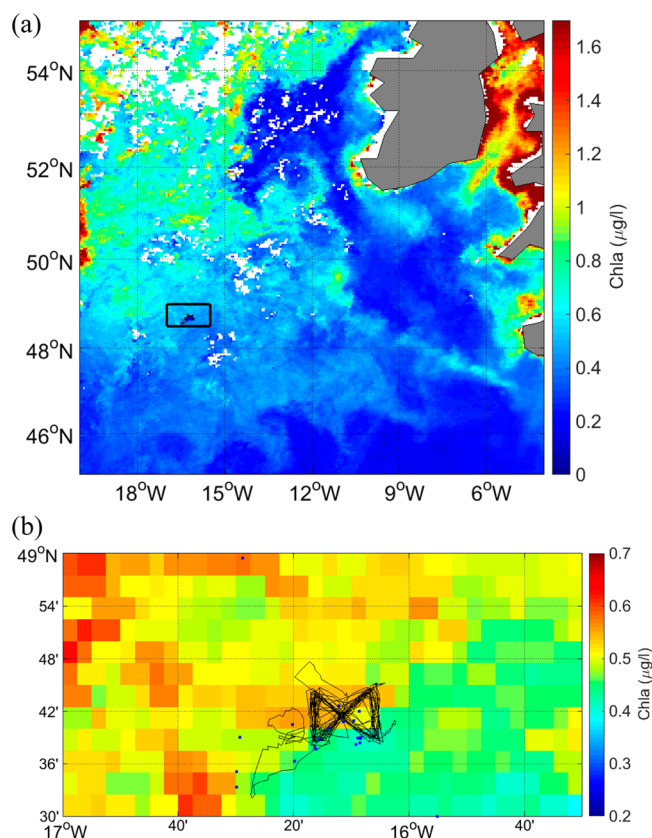
Figure 1. Modis aqua chlorophyll map showing location of study site and track of glider (black line) and CTD position (blue dots). The black box in (a) indicates the location of the expanded map (b).

2.2. Seaglider Data.

A Seaglider is an autonomous, buoyancy driven vehicle that profiles to a depth of 1000 m with a 0.5−1 m vertical sampling resolution along a sawtooth trajectory.[31−33] Seaglider SG566 was deployed from April to September 2013 sampling a 15 km × 15 km area, following a figure-of-eight path with an average 1000 m profiling time of 2.6 h for an up/down cast (Figure 1).

SG566 was equipped with an unpumped Seabird SBE13 CT sail (conductivity−temperature; Seabird Electronics, Bellevue, USA), a Paine pressure sensor (Paine Electronics, East Wenatchee, USA), a Triplet Ecopuck (Wetlabs, Philomath, USA) measuring chlorophyll fluorescence and optical back scatter, and a broadband 4π cosine photosynthetically active radiation (PAR) sensor (400−700 nm; Biospherical Instruments, San Diego, USA). Raw measurements from the CT sail were initially calibrated using manufacturer-supplied coefficients, with further corrections to account for thermal lag.[34] Glider salinities were calibrated against cruise data.[35] Pressure measurements were corrected to remove long-term drift and to account for pressure hysteresis within each dive.

Manufacturer calibrations were initially applied to data from the Wetlabs Triplet and 4π PAR by subtracting the instrument blank and applying a scaling factor. The manufacturer's calibration for chlorophyll fluorescence is based on the sensor's response to a culture of the phytoplankton species *Thalassiosira weissflogii* at a known chlorophyll-*a* concentration (Figure S3).[36] Our secondary calibration is outlined below. Other empirical methods have been developed to calibrate fluorescence profiles including ones that take into account the presence of an SCM,[20] but by using in situ PAR data, a scale factor can be

derived which can change dynamically and hence reflect changes in community composition (see Section 4.2). The manufacturer's PAR sensor calibration uses a traceable 1000 W type FEL Spectral Irradiance Standard. All data were aggregated into 2 m depth intervals.

To obtain estimates of PP, we used calibrated chlorophyll fluorescence, temperature, and PAR (Sections 2.5−2.7, Figure S1). Optical backscatter measurements were used to correct for fluorescence quenching,[37] and temperature, salinity, and density were used to estimate mixed layer depths.

2.3. In Situ Samples.

Three cruises to the survey region were conducted by the RRS *James Cook*: glider deployment (JC085; April 14−29), midmission (JC087; June 1−18), and glider recovery (JC090; September 1−16). Water samples for chlorophyll-*a* were collected on all cruises from up to six depths across the euphotic zone using a Seabird 911 plus CTD-Niskin rosette system. Chlorophyll-*a* concentrations were measured using 250 mL water samples filtered onto 25 mm Whatman glass fiber filters (GF/F; nominal pore size, 0.7 μm). Chlorophyll-*a* pigment was extracted in 6 mL of 90% acetone at 4 °C in the dark for ~20 h before measurement on a Turner Designs Trilogy fluorometer calibrated against a pure chlorophyll standard (spinach extract, Sigma Aldritch).[38] Two ship-fitted cosine collectors (Skye Instruments, UK) measured incident PAR.

Measurements of PP using the ^{13}C method[39] were made between 30th May and 18th June on JC087 only. Water samples were collected from predawn CTD casts at five depths: 55%, 20%, 7%, 5% and 1% of surface irradiance based on profiles obtained from previous midday CTD casts. Each 1 L water sample was added to an acid-rinsed Nalgene polycarbonate bottle, which was wrapped with optical filters (Lee Filters, Hampshire, UK) to replicate the appropriate irradiance levels. Each bottle was spiked with 200 μL of ^{13}C labeled sodium bicarbonate (0.65g in 50 mL of pH adjusted Milli-Q water), corresponding to an addition of 255 μmol L^{-1} (or ~1% of ambient (~2084 μmol L^{-1}) dissolved inorganic carbon concentrations). Sealed sample bottles were placed in on-deck incubators, which were flushed with surface seawater for 24 h. Afterward, each sample was filtered onto an ashed (450 °C, 6 h) 25 mm GF/F (Whatman) filter and rinsed with a weak HCl solution (1−2%) to remove inorganic carbon before being stored frozen at −20 °C. Filters were oven-dried and encapsulated in tin capsules. Samples were analyzed for ^{13}C isotopic enrichment at the Scottish Association for Marine Science using an ANCA NT preparation system coupled to a PDZ 20-20 Stable Isotope Analyzer (PDZ Europa Scientific Instruments, UK). PP was calculated from the stable isotope results using standard equations.[40]

2.4. Satellite Ocean Color Data and Primary Production Estimates.

We obtained 1 km resolution daily chlorophyll composites of MODIS Aqua data from the NERC Earth Observation Data Acquisition and Analysis Service (NEO-DAAS). For each Seaglider surfacing, the satellite data pixel that matched the position and date was extracted. Cloud cover resulted in data gaps in satellite coverage and surface match ups; these time periods were omitted from the analysis.

Full depth profiles of chlorophyll were calculated for satellite data using statistical relationships relating satellite chlorophyll to the shape of the chlorophyll profile at depth (Supporting Information).[14] For an alternative estimate of PP, for comparison to the glider-based estimates, these profiles and surface PAR were inputs to a PP algorithm[41] that couples the glider photosynthesis model[42] (Section 3.3) to the HYDROLIGHT radiative transfer
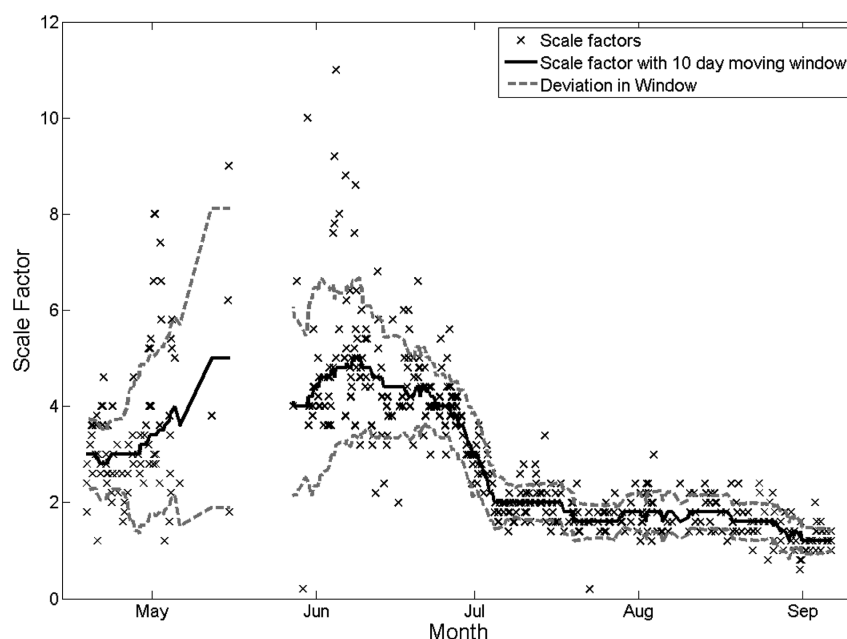
Figure 2. Scale factors calculated by optimization of modeled attenuation of irradiance against measured attenuation of irradiance (black ×) with the 10 day moving window (black line) and the standard deviation for each moving window (gray dashed line). The tick marks on the *x*-axis represent the beginning of each month.

code[43] which uses sea surface temperature, PAR, and day length to more accurately estimate irradiance with depth.

2.5. Irradiance Corrections, Calibrations, and Calculation. PP is best parametrized using spectral irradiance, as shorter wavelengths are absorbed much faster than long wavelengths; therefore, blue light penetrates much deeper into the water column.[44] Nonspectral methods can overestimate PP by as much as 50% if only broadband PAR is used.[10] A number of calculations are necessary to spectrally resolve the glider broadband PAR observations.

The glider only records subsurface PAR, so we first estimate surface irradiance for comparison with a surface irradiance model. We then decompose the surface irradiance into spectral components. Irradiance at depth was calculated using spectrally weighted algorithms.[46] Details are described below.

SG566 returned 1325 profiles of chlorophyll and PAR (downcast and upcast counted separately). Profiles where PAR intensity increased with depth (due to passing cloud cover and/or glider rolls)[46] were excluded from the analysis (319). We also excluded night-time profiles (417) leaving a total of 589 simultaneous profiles for analysis.

2.5.1. Estimating Surface Irradiance from Subsurface Glider Measurements. The fraction of solar irradiance entering the water column depends on the amount of sunlight reflected by the sea surface. This is calculated by separating the diffuse and direct components of irradiance using determinations of the Fresnel reflectance and the amount of foam (see Supporting Information). The total reflectance (r_{tot}) is the sum of direct reflectance (r_d) and diffusive reflectance (r_{diff}).

$$r_{tot} = r_d + r_{diff} \tag{1}$$

Glider PAR was extrapolated to just below the surface by assuming exponential attenuation. The following equation was then applied to calculate PAR just above the surface, $E(0^+)$

$$E(0^+) = \frac{E(0^-)(1 - R\bar{r})}{(1 - r_{tot})} \tag{2}$$

where $E(0^-)$ is the irradiance just below the surface and R is the irradiance reflectance (usually <0.1 in ocean waters). The water–air Fresnel reflection for the whole diffuse upwelling radiation ($\bar{r}$) has a value of 0.48.[44] R and $\bar{r}$ are needed to obtain the upwelling irradiance flux, which is subsequently reflected back down upon reaching the water surface.[44]

2.5.2. Calculating Spectral Irradiance. Surface PAR from the Seaglider (eq 2) was spectrally decomposed into 5 nm wavelengths, $E_0(\lambda)$, using a look-up table[41] created by generating a clear sky run of a radiative transfer model,[47] which is specific for oceanographic applications and adapted to include the effects of cloud cover.[48] For a given day, this model is run for noon using the glider surfacing position and relevant meteorological parameters to attenuate irradiance through the atmosphere (British Atmospheric Data Centre, BADC). The model outputs a spectrally resolved, full day irradiance time series just above the surface of the ocean for the location of interest. The integrated irradiance over all wavelengths for the time of the glider measurements was calculated in μmol quanta m^{-2} s^{-1}. The ratio between $E(0^+)$ from eq 2 and the integrated clear sky run is used to scale the spectral values for the day in question using each profile in that day to get spectral irradiance over the whole day at half hour intervals.

2.5.3. Spectral Irradiance through the Water Column. To calculate spectral irradiance ($E(z,\lambda)$) at a given depth in the water column, we used the equation,[49]

$$E(z, \lambda) = E_0(\lambda) \int_z^0 \exp([-K_w(\lambda) + K_c(\lambda)]z) \tag{3}$$

where $K_w(\lambda)$ is the attenuation coefficient associated with water and $K_c(\lambda)$ is the attenuation coefficient associated with chlorophyll and other dissolved material at specific wavelengths, λ. Morel and Maritorena[45] calculate $K_c(\lambda)$ as

$$K_c(\lambda) = \chi_c(\lambda)\mathrm{Chl}^{e(\lambda)} \tag{4}$$
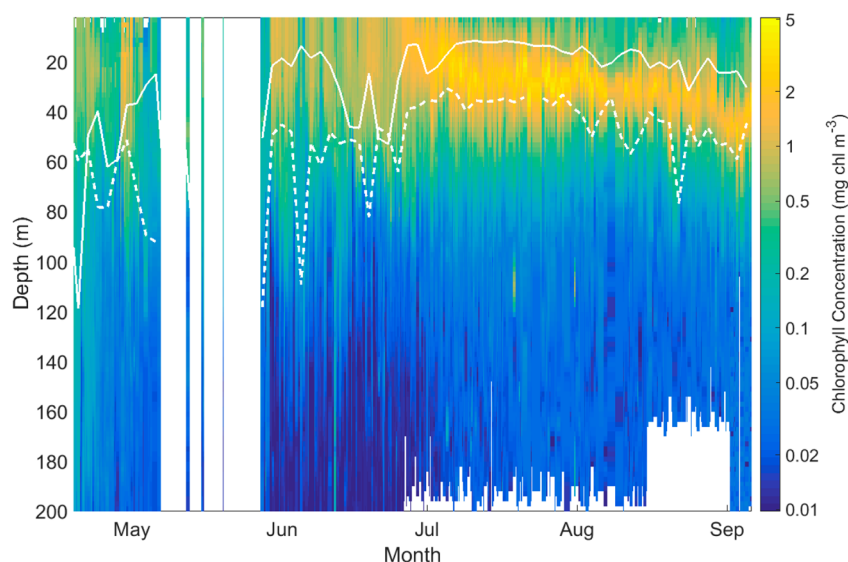
Figure 3. Time series of PAR corrected chlorophyll profiles; solid white line shows the mixed layer depth (m) and the dashed white line shows the euphotic depth (m), calculated from the glider PAR profiles.

The coefficient χ_c and the exponent $e(\lambda)$ are both functions of wavelength, and Chl is chlorophyll concentration (mg m^{-3}). Wavelengths within the PAR broadband range are used at 5 nm intervals.

2.6. Chlorophyll Corrections and Calibrations. As the manufacturer's calibration is often insufficient,[20,50] a number of steps are carried out to calibrate the chlorophyll estimates. First, the fluorescence data is corrected for quenching. Second, a scale factor for chlorophyll fluoresence is estimated by comparing modeled to observed irradiance attenuation. Details are given below (Figure 1).

2.6.1. Quenching Corrections. Daytime chlorophyll fluorescence exhibited fluorescence quenching in the top 20 m with low fluorescence during high irradiance. To correct for quenching, we have used the night-time relationship between fluorescence and optical backscatter (see Supporting Information for details).[38,51] We call the result the uncorrected-chlorophyll.

2.6.2. PAR-Based Chlorophyll Calibrated. We calibrated the chlorophyll fluorescence sensor using the PAR measurements and eq 3[49] to model the irradiance attenuation due to chlorophyll.[46] The uncorrected-chlorophyll profile (with dives and climb treated separately) was divided by a scaling factor ranging from 0.2 to 25 in intervals of 0.2, and the spectral irradiance profile was recalculated for each value based on the resulting scaled chlorophyll concentration profile and surface irradiance (eqs 3 and 4). Modeled values of spectral irradiance were then integrated over all wavelengths (400−700 nm) to compare to glider PAR measurements. A root mean squared error (RMSE) was calculated between the modeled and measured PAR values, over all depths (typically 50 points), for each scale factor.

For each profile, the scale factor with the lowest RMSE was then used to scale the uncorrected-chlorophyll concentration. This approach produces an independent scaling factor for each dive/climb, allowing for drift in the fluorometer to be corrected. The method assumes Case I water characteristics where CDOM and particulates covary with phytoplankton.[51,52] This method can be used if the glider PAR sensor is uncalibrated provided the

fluorescence-chlorophyll relationship is linear as we are only calculating attenuation rather than absolute PAR.

Variation in the scaling factor over a deployment period may result from poorly resolved PAR profiles (e.g., significant glider rolls or cloud cover). Profile-to-profile variability was reduced by using the median scaling factor calculated for a 10-day moving window. A 10-day window was picked arbitrarily, but no significant difference was seen using 6, 8, or 10 days. Longer time intervals resulted in oversmoothing of the scaling factor.

Final PAR-corrected chlorophyll concentrations for each profile were obtained using the appropriate 10-day median scale factor (Figure 2). These calibrated chlorophyll profiles (Figure 3) were used as input into the PP model, along with the spectral downwelling PAR (Section 3.1).

2.7. Calculating Primary Production. PP was calculated with the glider profiles of irradiance and PAR-corrected chlorophyll using depth, time, and wavelength-resolved irradiance.[42] PP is represented by a triple integral, integrating over day length (L), depth (D), and wavelength (λ) from $\lambda_1 = 400$ nm to $\lambda_2 = 700$ nm,

$$PP = 12 \int_0^L \int_0^D \int_{\lambda_2}^{\lambda_1} Chl(Z) PAR(\lambda, Z, t) a^*(\lambda) \phi_\mu(\lambda, Z, t) \, d\lambda \, dZ \, dt$$

(5)

where a^* is the absorption cross section per unit of chlorophyll (m^{-1}) and ϕ_μ is the net growth rate (mol C (mol quanta)$^{-1}$). These values are parametrized as in Morel et al.[54] (see Supporting Information for details). Each separate dive and climb were assigned an average time and position (latitude and longitude) for the profile. The model requires surface downwelling spectral irradiance (Wm^{-2} nm^{-1}), which is provided by the glider PAR sensor (Section 3.1.2).

3. RESULTS

3.1. Glider Chlorophyll. *3.1.1. PAR-Corrected Chlorophyll Data.* The scale factor used to calibrate the chlorophyll data (Figure 2) has a mean of 3 (range of 0.6−11). In May, there is a peak of 5 but only 4 profiles were used to calculate this scale factor (range of 1.2−8.8), as the sensors were turned off for a time to save battery, so it is not as well constrained as in other months when more profiles were available. Starting in July, the

scale factor was less variable (range of 1.2−1.8) for the remainder of the deployment.

The chlorophyll profiles are shown in Figure 3 for the whole deployment period. Concentrations were <1.5 mg Chl-*a* m^{-3} from May until July, when they increased to >2 mg Chl-*a* m^{-3}. Before July, the chlorophyll concentration varied little within the top 30 m. A SCM started to form toward the end of July, with maximum chlorophyll concentrations >4 mg Chl-*a* m^{-3} at a depth of 30 m. Surface concentrations during August were very low, <0.6 mg Chl-*a* m^{-3}. By the end of August, the SCM deepened to 40 m and maximum concentrations in the SCM decreased to <2.5 mg Chl-*a* m^{-3}, with surface concentrations <0.4 mg Chl-*a* m^{-3}.

3.1.2. Comparison of Glider and Bottle-Sample Estimates of Chlorophyll. Figure 4 compares discrete bottle-sample chlorophyll and PAR-corrected glider chlorophyll for the 3 cruises. In late April (JC085) and prior to the spring bloom, the discrete chlorophyll concentrations were comparable to the PAR-corrected chlorophyll concentrations. Surface concentrations ranged from 0.25 to 0.7 mg Chl-*a* m^{-3} and 0.15 to 0.8 mg Chl-*a* m^{-3} for the discrete samples and glider estimates, respectively. The range in glider-based chlorophyll concentrations was slightly larger, likely due to the greater number of glider profiles detecting a wider range of concentrations. At depths between 75 and 150 m, bottle samples were approximately 0.1−0.2 mg Chl-*a* m^{-3} higher than the glider, which effectively measured close to zero at these depths, which is below the euphotic depth (60 m).

In June, the majority of discrete chlorophyll measurements were elevated compared to the glider estimates, particularly throughout the upper 50 m. Surface concentrations ranged from 0.05 to 1.2 mg Chl-*a* m^{-3} for the glider compared with 0.08 to 1.8 mg Chl-*a* m^{-3} from bottle samples (Figure 4). There was no offset between the glider and discrete measurements below 75−150 m, suggesting no systematic error. Chlorophyll values below 100 m were <0.4 mg Chl-*a* m^{-3}, with the majority of the glider and discrete measurements <0.2 mg Chl-*a* m^{-3}.

For the final cruise in September (JC90), discrete and glider chlorophyll estimates were comparable (Figure 4). Surface values ranged between 0.4 and 1 mg Chl-*a* m^{-3} in the discrete water samples, whereas the glider chlorophyll ranged from <0.1 to 0.75 mg Chl-*a* m^{-3}. A SCM around 40 m was measured by both data sets, with similar maximum values (3.3 mg Chl-*a* m^{-3}).

The lateral distances between CTD and glider profiles were compared with the differences in surface chlorophyll concentrations (Figure S4, Spearman[55] $R^2 = 0.53$, $p < 0.001$, $n = 19$). Surface chlorophyll differences decrease with distance, suggesting that spatial differences remain an important consideration in the comparison of glider and in situ data. Many of the CTD profiles were located >30 km away from the glider making it possible that spatial variability associated with the onset of the spring bloom at this time affects the comparison. This is also consistent with the glider data, which can show significant variations in water mass properties and chlorophyll concentrations along a single 15 km transect. Cloud cover hinders examining this from satellite images in more detail.

3.2. Depth Integrated Primary Production. *3.2.1. Depth Integrated Glider Estimates of Primary Production.* Glider-based estimates of PP ranged from 0.38 to 30 g C m^{-2} d^{-1} over the 5 months, displaying strong temporal variability. These estimates have been compared to ship-based ^{13}C measurements and 1 km satellite estimates (Figure 5).
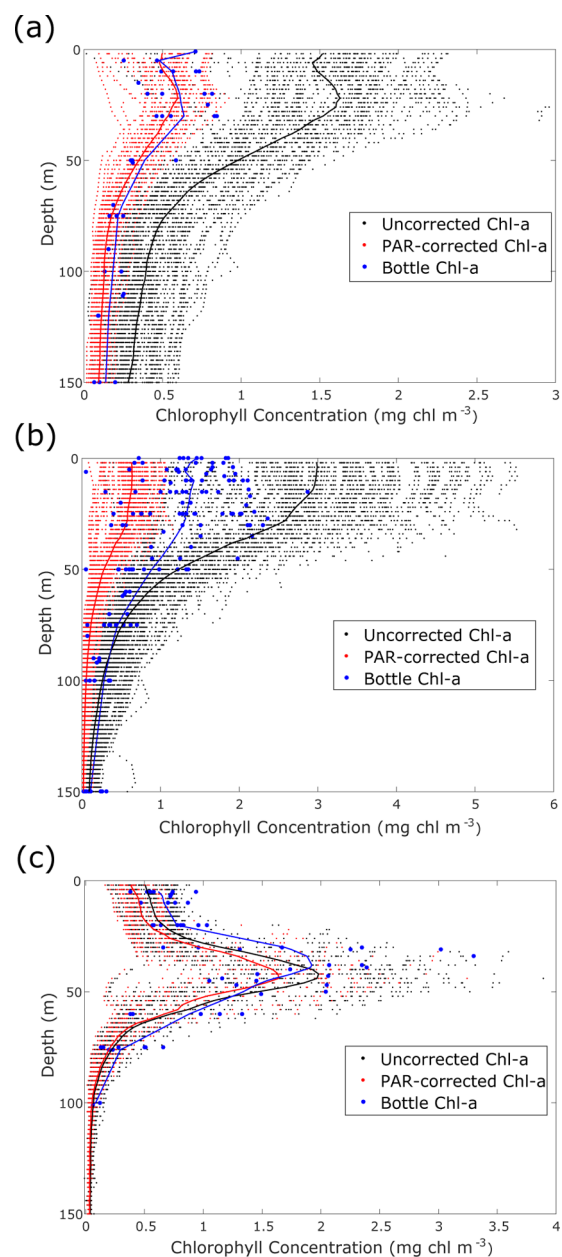

(a)

(b)

(c)

Figure 4. Glider profiles of chlorophyll, uncorrected and PAR-corrected, compared to ship-based bottle samples of chlorophyll from acetone extracts. Mean profiles are shown as solid lines. For cruises (a) JC85, (b) JC87, and (c) JC90.

The ^{13}C PP estimates from June are compared to glider estimates in Figure 5a. Glider profiles on the same day were averaged together for comparison. ^{13}C PP increased from the 6th to 14th of June, with values ranging from 0.5 to 1.9 g C m^{-2} d^{-1}, whereas the glider estimates of PP were relatively consistent, varying from 1.1 to 1.6 g C m^{-2} d^{-1} over the same time period. Glider PP measurements were higher on average by 0.17 g C m^{-2} d^{-1} (or 39%), but offsets were also highly variable (Figure 5a).

PP estimates obtained using the uncorrected-chlorophyll profiles are also presented in Figure 5a. On average, this resulted in productivity estimates over 2-fold higher than the ^{13}C observations.

In Figure 5b, we present a time series of water column integrated PP over the five month glider deployment, in conjunction with ^{13}C measurements already shown in Figure
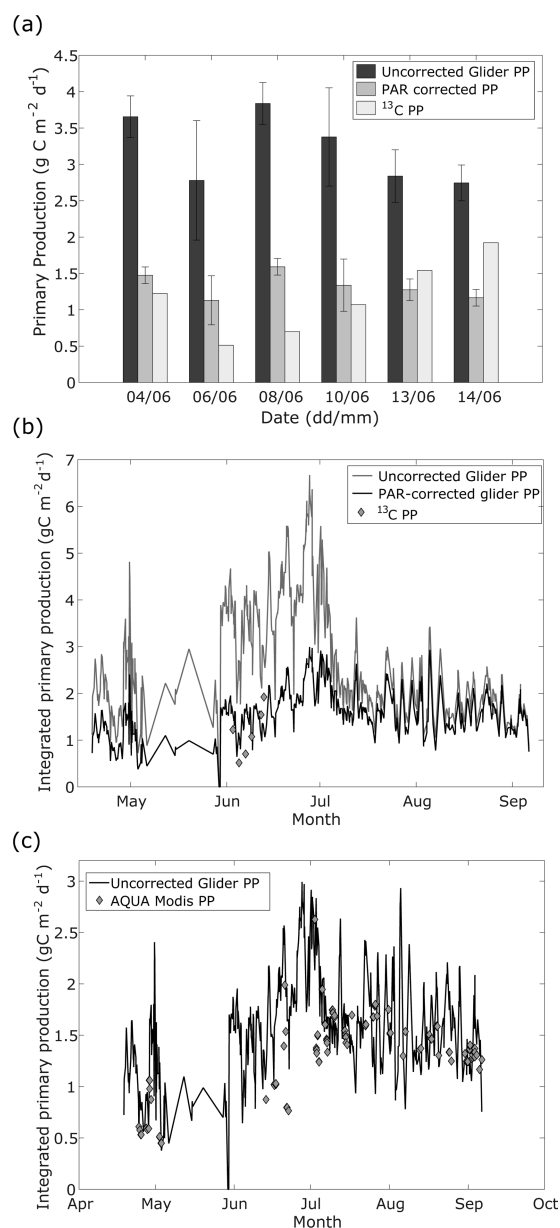
5a. The glider estimates were higher than the ^{13}C measurements but not unreasonably so. Integrated PP rates from late April to May were ~1 g C m^{-2} d^{-1} increasing to a maximum of 3 g C m^{-2} d^{-1} in July. Toward the end of July and through August, rates decreased to 1.5 g C m^{-2} d^{-1} but remained highly variable, fluctuating by ±0.6 g C m^{-2} d^{-1}. Due to the high level of cloud cover, there were no satellite pixel matches during the time period when the in situ measurements were taken and therefore a comparison with satellite and ship-based measurements was not possible.

Integrated PP estimates from the glider and satellite were also compared (Section 2.3, Figure 5c). The correlation between the satellite and glider estimates of surface PP was modest but nevertheless statistically significant (Figure S5; Spearman[55] R^2 = 0.322, $p < 0.0001$, $n = 122$). In general, the glider shows higher integrated estimates of PP than the satellite. Dissimilarity between estimates is likely due to differences in the PAR values and between the modeled and observed SCM. The mean root mean squared error between the modeled and observed chlorophyll profiles was 0.9 mg Chl-a m^{-3} (range of 0.58−1.36 mg Chl-a m^{-3}).

Figure 5c shows that the satellite and glider have reasonably good agreement during the deployment with similar variability, trends, and magnitude in PP. Both data sets show an increase in production from May to June (spring bloom) and a production maximum in July, with maximum rates of 3 and 2 g C m^{-2} d^{-1} decreasing again in late July, for the glider and satellite, respectively, although glider estimates of PP are on average 16% higher than satellite estimates.

3.2.2. Glider Estimates of Seasonal Primary Production vs Literature Estimates. Due to the limited number of ^{13}C in situ measurements, we also present a comparison with productivity estimates from the literature for the same region (Table 1).[25,56−59] The literature values span 0.3−2 g C m^{-2} d^{-1}, comparable with our ^{13}C measurements. However, toward the end of June and July, the literature observations are lower than those estimated from the glider and our ^{13}C measurements. This may be interannual variability. Overall, our ^{13}C values are within the range of literature values supporting the use of this data to compare to the glider estimates.

3.3. Depth Resolved Primary Production. Depth resolved PP over the deployment (Figure 6) shows that throughout May and June PP was highest at the surface and decreased with depth due to irradiance attenuation. In July, as chlorophyll and irradiance concentrations increased, PP also increased with maximum surface rates of 0.45 g C m^{-3} d^{-1}. In late July, a subsurface production maximum formed with PP rates of 0.2−0.3 g C m^{-3} d^{-1}. The production maximum deepened throughout August from 15 to 30 m. The productivity maximum was located just beneath the mixed layer but also below the optical sampling depth for remote sensing.

Figure 5. (a) Daily mean PP from Seaglider dives compared with in situ ^{13}C estimates of production. Error bars are the standard deviation of the PP calculated from all the dives in 1 day. Water samples for the incubations were taken at dawn, a 12 h day for production is assumed. (b) Differences between integrated PAR-corrected glider primary production and the uncorrected glider primary production compared with ^{13}C primary production measurements. (c) Primary production estimates for the duration of glider deployments for SG566 and NEODAAS 1 km daily product.

Table 1. Mean Productivity Rates from the NE Atlantic as Reported in the Literature[a]

reference	sampling period	position	integration depth (m)	n	mean (±standard deviation) (g C m^{-2} d^{-1})
this study	June 2013	48°N 16°W	euphotic zone	6	1.16 (0.5)
Chipman et al., (1993)[56]	May 1989	47°N 20°W	euphotic zone	11	0.84 (0.19)
Marra et al., (1995)[57]	June 1991	59.5°N 21°W	euphotic zone	4	1 (0.46)
Savidge et al., (1995)[58]	May/June 1990	47−60°N 20°W	euphotic zone	25	0.70 (0.32)
Bury et al., (2001)[59]	May 1990	47°N 20°W	euphotic zone	8	0.84 (0.50)
Painter et al., (2010)[25]	July 2006	49°N 16°W	euphotic zone	3	0.55 (0.22)

[a]All estimates were made using the ^{13}C stable isotope method.
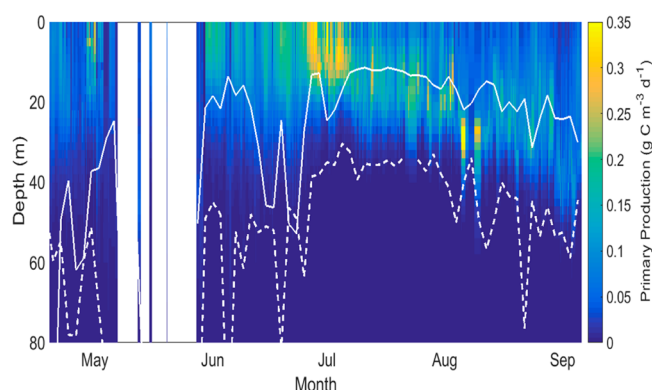
Figure 6. Time series of PAR-corrected primary production profiles for SG566 for the entire deployment; the solid white line is the mixed layer depth (m), and the dashed white line is the euphotic depth (1% of surface irradiance levels).

The euphotic depth was 60−80 m throughout May and June, with variable mixed layer depths (MLD) of between 40 and 130 m. The euphotic depth shoaled to 35 m in July coincident with increasing chlorophyll concentrations and greater irradiance attenuation[53] and a shoaling of the MLD due to either surface forcing (heating) or a restratification through physical processes such as Ekman transport, mixed layer instabilities, and lateral advection. The subsurface production maximum in late July and August was around the same depth as the mixed layer. However, the SCM was deeper than the production maximum by 10 m and below the mixed layer, suggesting that the SCM was preferentially located where nutrient concentrations were higher. In August, the SCM was located between the MLD and the euphotic depth (Figure 3).

Depth profiles of the ^{13}C productivity measurements are shown in Figure S6 alongside the range and mean of the coincident glider profiles. Although the ^{13}C productivity rates were lower than the mean glider profile, they lie mostly within the range of glider data. Some of the ^{13}C profiles show a production maximum around 30 m whereas the glider estimated profiles do not. Two profiles also show higher production at depth than that estimated from the glider.

4. DISCUSSION

4.1. Advantages of Calculating Primary Production Using Gliders. Fine scale measurements are important since submesoscale features are often present, such as highly productive filaments.[25] Furthermore, PP may change over daily time scales due to changes in irradiance and mixed layer depth. Such short time scales (hours) are not resolved by remote sensing, but with several profiles a day, a glider can observe these changes. Early June showed differences in integrated production rates between sequential dives of 0.3 and 1 g C m^{-2} d^{-1}. The average daily production was <2 g C m^{-2} d^{-1}, so this difference was significant. Small scale temporal variations in PP may be important in determining the carbon budget,[25] especially in areas of high variability of phytoplankton.

A key advantage of using gliders is the ability to resolve subsurface features, previously only possible using ship-based measurements. Satellite production estimates are only resolved to the first optical depth, and it has been shown that including fluorescence profiles significantly improves estimates.[12] Knowing the distribution of chlorophyll at depth is considered vital for ecological studies.[60] Glider production rates were 16% higher

than satellite estimates during the deployment suggesting that satellite-based estimates of production may be slightly under-estimating PP during summer months in this region. Subsurface chlorophyll maxima contribute significantly to integrated PP in temperate latitudes so implementation of subsurface glider profiles will improve regional estimates.[61] Subsurface production maxima are common globally, and this contribution is often modeled incorrectly for specific regions when using satellite color to estimate PP.[15,62,63] Therefore, gliders have considerable potential to improve satellite estimates of PP.[12]

Gliders also have the benefit of being able to continuously sample in all weather conditions. Ship-based measurements are weather and time dependent. Satellite coverage is restricted by cloud cover, which can introduce sampling bias.[64,65] During this deployment, 467 profiles out of 589 (79%) had no direct satellite matchup due to high levels of cloud cover, equating to a loss of 105 days of satellite coverage over the whole deployment of 141 days. Using 1 km pixel match ups is a strong constraint impacting the number of match-ups.

4.2. Limitations of Glider Estimated Primary Production. The spectral constants for chlorophyll used in the irradiance attenuation calculations (eq 4) differ compared to other literature values due to regional differences in community composition and/or temperature.[66,67] Additional uncertainty is introduced when broadband PAR is split spectrally. The method assumes that clouds, changes in atmospheric absorption, and season influence spectral values of PAR linearly.[41] The photosynthetic rate per unit of biomass (eq 5) remains the largest unknown in the PP algorithm because of its high variability in the ocean.[68]

Fluorescence measurements, which are only a proxy for chlorophyll-*a*, can be difficult to interpret. The fluorescence yield per unit of chlorophyll is known to change in response to changes in community structure.[69] The changing scale factor used to calibrate glider chlorophyll and the rapid decrease in the scale factor seen in July (Figure 2) may therefore be indicative of postbloom changes to the community composition. We cannot verify this with the data available. However, using a time-dependent scale factor to probe community structure would be an interesting topic to explore.

Measurements from autonomous platforms present their own challenges. Sensor calibrations may drift with time or with biofouling.[18] Additional calibration measurements collected at deployment and recovery could indicate this. For this deployment, no biofouling was noted at recovery and there was no drift in dark counts at depth, so fouling is unlikely. Discrepancies were seen between bottle data and the PAR-corrected glider chlorophyll. As few CTD casts were made near the glider and this area is known to display patchy chlorophyll distributions,[25] comparisons can be complicated. However, the data are broadly consistent suggesting that glider productivity rates are generally appropriate for the region.

4.3. Future Applications. While we have used gliders to quantify PP in a region of the North Atlantic, this approach will allow improved estimates of PP more widely in the future, particularly in regions with SCMs and/or considerable cloud cover. We have demonstrated the suitability of gliders for capturing fine-scale temporal changes in production at daily time scales over a single season. Gliders allow coincident and simultaneous measurements of physical parameters, including density, temperature, oxygen, and vertical water velocity.[70,71] The coincident analysis of the physical environment allows an improved understanding of influences on phytoplankton growth.

Small-scale physical processes may account for a significant amount of new production.[50,72,73] Several recent studies have used high resolution data from gliders to analyze biological and physical connections.[74−78] Simultaneous estimates of PP will further resolve biological and physical connections.

■ ASSOCIATED CONTENT

Ⓢ Supporting Information

The Supporting Information is available free of charge on the ACS Publications website at DOI: 10.1021/acs.est.5b00608.

> Extended methods, specifically quenching corrections, validation of PAR and surface irradiance calculations, and Figures S1−S6 (PDF)

■ AUTHOR INFORMATION

Corresponding Author
*E-mail: vsh1g12@soton.ac.uk.

Notes
The authors declare no competing financial interest.

■ ACKNOWLEDGMENTS

■ REFERENCES

(1) Carr, M. E.; Friedrichs, M. A. M.; Schmeltz, M.; Aita, M. N.; Antoine, D.; Arrigo, K. R.; Asanuma, I.; Aumont, O.; Barber, R.; Behrenfeld, M.; Bidigare, R.; Buitenhuis, E. T.; Campbell, J.; Ciotti, A.; Dierssen, H.; Dowell, M.; Dunne, J.; Esaias, W.; Gentili, B.; Gregg, W.; Groom, S.; Hoepffner, N.; Ishizaka, J.; Kameda, T.; Le Quéré, C.; Lohrenz, S.; Marra, J.; Mélin, F.; Moore, K.; Morel, A.; Reddy, T. E.; Ryan, J.; Scardi, M.; Smyth, T.; Turpie, K.; Tilstone, G.; Waters, K.; Yamanaka, Y. A comparison of global estimates of marine primary production from ocean color. *Deep Sea Res., Part II* **2006**, *53* (5−7), 741−770.

(2) Field, C. B. Primary Production of the Biosphere: Integrating Terrestrial and Oceanic Components. *Science* **1998**, *281* (5374), 237−240.

(3) Parekh, P.; Follows, M. J.; Dutkiewicz, S.; Ito, T. Physical and biological regulation of the soft tissue carbon pump. *Paleoceanography* **2006**, *21*, PA3001.

(4) Nightingale, P. D.; Malin, G.; Law, C. S.; Watson, A. J.; Liss, P. S.; Liddicoat, M. J.; Boutin, J.; Upstill-Goddard, R. C. In situ evaluation of air-sea gas exchange parameterizations using novel conservative and volatile tracers. *Global Biogeochemical Cycles* **2000**, *14* (1), 373−387.

(5) Wanninkhof, R. Relationship between wind speed and gas exchange over the ocean. *J. Geophys. Res.* **1992**, *97* (C5), 7373−7382.

(6) Liss, P. S.; Merlivat, L. Air-sea gas exchange rates: Introduction and synthesis. In *The Role of Air-Sea Exchange in Geochemical Cycling*; Buat-Ménart, P., Ed.; D. Reidel Pub. Co.: Norwell, MA, 1986; pp 113−129.

(7) Eppley, R. W.; Stewart, E.; Abbott, M. R.; Heyman, U. Estimating ocean production from satellite chlorophyll: introduction to regional difference and statistics in the southern California bight. *J. Plankton Res.* **1985**, *7* (1), 57−70.

(8) Bidigare, R. R.; Smith, R. C.; Baker, K. S.; Marra, J. Oceanic primary production estimates from measurements of spectral irradiance and pigment concentrations. *Global Biogeochemical Cycles* **1987**, *1* (3), 171−186.

(9) Platt, T.; Sathyendranath, S. Oceanic primary production: estimation by remote sensing at local and regional scales. *Science* **1988**, *241* (4873), 1613−1620.

(10) Sathyendranath, S.; Platt, T.; Caverhill, C.; Warnock, R.; Lewis, M. Remote sensing of oceanic primary production: computations using a spectral model. *Deep-Sea Res., Part A* **1989**, *36* (3), 431−453.

(11) Behrenfeld, M. J.; Falkowski, P. G. A consumer's guide to phytoplankton primary productivity models. *Limnol. Oceanogr.* **1997**, *42*, 1479−1491.

(12) Jacox, M. G.; Edwards, C.; Kahru, M.; Rudnick, D. L.; Kudela, R. M. The potential for improving remote primary productivity estimates through subsurface chlorophyll and irradiance measurement. *Deep Sea Res., Part II* **2015**, *112*, 107−116.

(13) Gordon, H. R.; Clark, K. Remote sensing optical properties of a stratified ocean: an improved interpretation. *Appl. Opt.* **1980**, *19* (20), 3428−3430.

(14) Morel, A.; Berthon, J. Surface pigments, algal biomass profiles and potential production of the euphotic layer: relationships reinvestigated in view of remote-sensing applications. *Limnol. Oceanogr.* **1989**, *34*, 1545−1562.

(15) Cullen, J. J. Subsurface chlorophyll maximum layers: enduring enigma or mystery solved. *Annual Review of Marine Science* **2015**, *7*, 207−239.

(16) Eriksen, C. C.; Perry, M. J. *The Nurturing of Seagliders by the National Oceanographic Partnership Program*; School of Marine Sciences at DigitalCommons@UMaine, 2009; Marine Sciences Faculty Scholarship, Paper 133.

(17) Rudnick, D. L.; Cole, S. T. On sampling the ocean using underwater gliders. *J. Geophys. Res.* **2011**, *116*, C08010.

(18) Perry, M. J.; Sackmann, B. S.; Eriksen, C. C.; Lee, C. M. Seaglider observations of blooms and subsurface chlorophyll maxima off the Washinton coast. *Limnol. Oceanogr.* **2008**, *53* (5, part 2), 2169−2179.

(19) Lorenzen, C. J. A method for the continuous measurement of in vivo chlorophyll concentration. *Deep-Sea Res. Oceanogr. Abstr.* **1966**, *13*, 223−227.

(20) Mignot, A.; Claustre, H.; D'Ortenzio, F.; Xing, X.; Poteau, A.; Ras, J. From the shape of the vertical profile of in vivo fluorescence to Chlorophyll-a concentration. *Biogeosciences* **2011**, *8*, 2391−2406.

(21) Lampitt, R. S.; Favali, P.; Barnes, C. R.; Church, M. J.; Cronin, M. F.; Hill, K. L.; Kaneda, Y.; Karl, D. M.; Knap, A. H.; McPhaden, M. J.; Nittis, K. A.; Priede, I. G.; Rollin, J.-F.; Send, U.; Teng, C.-C.; Trull, T. W.; Wallace, D.W. R.; Weller, R. A. In situ sustained Eulerian observatories. In *Proceedings of OceanObs'09: Sustained Ocean Observations and Information for Society, Vol. 1. OceanObs'09: Sustained Ocean Observations and Information for Society*, Noordwijk, The Netherlands, European Space Agency, 2010; Hall, J., Harrison, D. E., Stammer, D., Eds.; pp 395−404 (ESA Special Publication WPP-306).

(22) Hartman, S. E.; Lampitt, R. S.; Larkin, K. E.; Pagnani, M.; Campbell, J.; Gkritzalis, T.; Jiang, Z.-P.; Pebody, C. A.; Ruhl, H. A.; Gooday, A. J.; Bett, B. J.; Billett, D. S. M.; Provost, P.; McLachlan, R.; Turton, J. D.; Lankester, S. The Porcupine Abyssal Plain fixed-point sustained observatory (PAP-SO): variations and trends from the Northeast Atlantic fixed = point time-series. *ICES J. Mar. Sci.* **2012**, *69* (5), 776−783.

(23) Lampitt, R. S.; Bett, B. J.; Kiriakoulakis, K.; Popova, E. E.; Ragueneau, O.; Vangriesheim, A.; Wolff, G. A. Material supply to the abyssal seafloor in the Northeast Atlantic. *Prog. Oceanogr.* **2001**, *50*, 27−63.

(24) Hartman, S. E.; Larkin, K. E.; Lampitt, R. S.; Lankhorst, M.; Hydes, D. J. Seasonal and inter-annual biogeochemical variations in the Porcupine Abyssal Plain 2003−2005 associated with winter mixing and surface circulation. *Deep Sea Res., Part II* **2010**, *57* (15), 1303−1312.

(25) Painter, S. C.; Pidcock, R. E.; Allen, J. T. A mesoscale eddy driving spatial and temporal heterogeneity in the productivity of the euphotic zone of the northeast Atlantic. *Deep Sea Res., Part II* **2010**, *57* (15), 1281−1292.

(26) Barlow, R. G.; Mantoura, R. F. C.; Gough, M. A.; Fileman, T. W. Pigment signatures of phytoplankton composition in the northeast Atlantic during the 1990 spring bloom. *Deep Sea Res., Part II* **1993**, *40* (1/2), 459−477.

(27) Henson, S.; Lampitt, R.; Johns, D. Variability in phytoplankton community structure in response to the North Atlantic Oscillation and implications for organic carbon flux. *Limnol. Oceanogr.* **2012**, *57* (6), 1591−1601.

(28) Lochte, K.; Pfannkuche, O. Cyclonic cold-core eddy in the eastern North Atlantic. II. Nutrients, phytoplankton and bacterioplankton. *Mar. Ecol.: Prog. Ser.* **1987**, *39*, 153−164.

(29) Painter, S. C.; Lucas, M. I.; Stinchcombe, M. C.; Bibby, T. S.; Poulton, A. J. Summertime trends in pelagic biogeochemsity at the Porcupine Abyssal Plain study site in the notheast Atlantic. *Deep Sea Res., Part II* **2010**, *57* (15), 1313−1323.

(30) Smythe-Wright, D.; Boswell, S.; Kim, Y.-N.; Kemp, A. Spatio-temporal changes in the distribution of phytopigments and phytoplanktonicgroups at the Porcupine Abyssal Plain (PAP) site. *Deep Sea Res., Part II* **2010**, *57* (15), 1324−1335.

(31) Eriksen, C. C.; Osse, T. J.; Light, R. D.; Wen, T.; Lehman, T. W.; Sabin, P. L.; Ballard, J. W.; Chiodi, A. M. Seaglider: a long-range autonomous underwater vehicle for oceanographic research. *IEEE J. Oceanic Eng.* **2001**, *26* (4), 424−436.

(32) Rudnick, D. L.; Davis, R. E.; Eriksen, C. C.; Fratantoni, D. M.; Perry, M. J. Underwater Gliders for Ocean Research. *Mar. Technol. Soc. J.* **2004**, *38* (2), 73−84.

(33) Davis, R. E.; Eriksen, C. C.; Jones, C. P. Autonomous Buoyancy-Driven Underwater Gliders. In *The Technology and Applications of Autonomous Underwater Vehicles*; Griffiths, G., Ed.; Taylor and Francis: London, U.K., 2002.

(34) Garau, B.; Ruiz, S.; Zhang, W. G.; Pascual, A.; Heslop, E.; Kerfoot, J.; Tintoré, J. Thermal lag correction on Slocum CTD glider data. *Journal of Atmospheric and Oceanic Technology* **2011**, *28* (9), 1065−1071.

(35) Damerell, G. M.; Heywood, K. J.; Thompson, A. F. Ocean Glider Observations of the Seasonal Evolution of the Upper Ocean in the North-East Atlantic. *Geophys. Res. Lett.*, in preparation.

(36) *Wetlabs ECO fluorometers and scattering sensors*; User Manual 10/2014, Edition 4. http://wetlabs.com/sites/default/files/documents/WETLabs-ECOMaster=3en.pdf.

(37) Stramski, D.; Boss, E.; Bogucki, D.; Voss, K. J. The role of seawater constituents in light backscattering in the ocean. *Prog. Oceanogr.* **2004**, *61*, 27−56.

(38) Welschmeyer, N. Fluorometric analysis of chlorophyll a in the presence of chlorophyll b and pheopigments. *Limnol. Oceanogr.* **1994**, *39* (8), 1985−1992.

(39) Slawyk, G.; Collos, Y.; Auclair, J. C. The use of the 13C and 15N isotopes for the simultaneous measurement of carbon and nitrogen turnover rates in marine phytoplankton. *Limnol. Oceanogr.* **1977**, *22*, 925−932.

(40) Legendre, L.; Gosselin, M. Estimation of N and C uptakes rates by phytoplankton using 15N and 13C: revisiting the usual computation formulae. *J. Plankton Res.* **1997**, *19* (2), 263−271.

(41) Smyth, T. J.; Tilstone, G. H.; Groom, S. B. Integration of radiative transfer into satellite models of ocean primary production. *J. Geophys. Res.* **2005**, *110* (C10), C10014.

(42) Morel, A. Light and marine photosynthesis: a spectral model with geochemical and climatological implications. *Prog. Oceanogr.* **1991**, *26*, 263−306.

(43) Mobley, C. D. *Hydrologht 3.0 Users' Guide*; SRI International: Menlo Park, California, U.S.A., 1995.

(44) Kirk, J. T. O. *Light and Photosynthesis in Aquatic Ecosystems*; Cambridge University Press: Cambridge, U.K., 2011.

(45) Morel, A.; Maritorena, S. Bio-optical properties of oceanic waters: A reappraisal. *J. Geophys. Res.* **2001**, *106* (C4), 7163−7180.

(46) Xing, X.; Morel, A.; Clausre, H.; Antoine, D.; D'Ortenzio, F.; Poteau, A.; Mignot, A. Combined processing and mutual interpretation of radiometry and fluorimetry from automonous profiling Bio-Argo floats: Chlorophyll a retrieval. *J. Geophys. Res.* **2011**, *116*, C06020.

(47) Gregg, W.; Carder, K. A simple spectral solar irradiance model for cloudless maritime atmospheres. *Limnol. Oceanogr.* **1990**, *35* (8), 1657−1675.

(48) Reed, R. K. On estimating insolation over the ocean. *Journal of Physical Oceanography* **1977**, *7*, 482−485.

(49) Carr, M. R. Modelling the Attenuation of Broad Band Light Down a Water Column. *Journal of the Royal Statistical Society, Series D (The Statistician)* **1986**, *35* (3), 325−33.

(50) Frajka-Williams, E.; Rhines, P. B.; Eriksen, C. Physical controls and Mesoscale variability in the Labrador Sea spring phytoplankton bloom observed by Seaglider. *Deep Sea Res., Part I* **2009**, *56*, 2144−2161.

(51) Boss, E.; Swift, D.; Taylor, L.; Brickley, P.; Zaneveld, R.; Riser, S.; Perry, M. J.; Strutton, P. G. Robotic in situ and satellite-based observations of pigment and particle distributions in the Western North Atlantic. *Limnol. Oceanogr.* **2008**, *53*, 2112−2122.

(52) Morel, A. Optical modelling of the upper ocean in relation to its biogenous matter content (case 1 water). *J. Geophys. Res.* **1988**, *93* (C9), 10749−10769.

(53) Bricaud, A.; Morel, A.; Babin, M.; Allali, K.; Claustre, H. Variations of light absorption by suspended particles with chlorophyll a concentration in oceanic (case 1) waters: Analysis and implications for bio-optical models. *J. Geophys. Res.* **1998**, *103*, 31033−31044.

(54) Morel, A.; Antoine, D.; Babin, M.; Dandonneau, Y. Measured and modelled primary production in the northeast Atlantic (EUMELI JGOFS program): the impact of natural variations in the photosynthetic parameters on model predictive skill. *Deep Sea Res., Part I* **1996**, *43* (8), 1273−1304.

(55) Spearman, C. The proof and measurement of association between two things. *Am. J. Psychol.* **1904**, *15*, 72−101.

(56) Chipman, D. W.; Marra, J.; Takahashi, T. Primary production at 47oN and 20oW in the North Atlantic Ocean: a comparison between the 14C incubation method and mixed layer carbon budget. *Deep Sea Res., Part II* **1993**, *40*, 151−169.

(57) Marra, J.; Langdon, C.; Knudson, C. A. Primary production, water column changes, and the demise of a Phaeocystis bloom at the Marine Light-Mixed Layers site (59° N, 21° W) in the northeast Atlantic Ocean. *J. Geophys. Res.* **1995**, *100* (C4), 6633−6643.

(58) Savidge, G.; Boyd, P.; Pomroy, A.; Harbour, D.; Joint, I. Joint, I. Phytoplankton production and biomass estimates in the northeast Atlantic Ocean, May−June 1990. *Deep Sea Res., Part I* **1995**, *42* (5), 599−617.

(59) Bury, S. J.; Boyd, P. W.; Preston, T.; Savidge, G.; Owens, N. J. P. Size-fractionated primary production and nitrogen uptake during a North Atlantic phytoplankton bloom: implications for carbon export estimates. *Deep Sea Res., Part I* **2001**, *48* (3), 689−720.

(60) Uitz, J.; Claustre, H.; Morel, A.; Hooker, S. B. Vertical distribution of phytoplankton communities in open ocean: An assessment based on surface chlorophyll. *J. Geophys. Res.* **2006**, *111*, C08005.

(61) Anderson, G. C. Subsurface chlorophyll maximum in the northeast Pacific Ocean. *Limnol. Oceanogr.* **1969**, *14*, 386−391.

(62) Weston, K.; Fernand, L.; Mills, D. K.; Delahunty, R.; Brown, J. Primary production in the deep chlorophyll maximum of the central North Sea. *J. Plankton Res.* **2005**, *27* (9), 909−922.

(63) Martin, J.; Tremblay, J.; Gagnon, J.; Tremblay, G.; Lapoussière, A.; Jose, C.; Poulin, M.; Gosselin, M.; Gratton, Y.; Michel, C. Prevalence, structure and properties of subsurface chlorophyll maxima in Canadian Arctic waters. *Mar. Ecol.: Prog. Ser.* **2010**, *412*, 69−84.

(64) Longhurst, A.; Sathyendranath, S.; Platt, T.; Caverhill, C. An estimate of global primary production in the ocean from satellite radiometer data. *J. Plankton Res.* **1995**, *17* (6), 1245−1271.

(65) Gregg, W. W.; Casey, N. W. Sampling biases in MODIS and SeaWiFS ocean chlorophyll data. *Remote Sensing of Environment* **2007**, *111* (1), 25−35.

(66) Carder, K. L.; Chen, F. R.; Lee, Z. P.; Hawes, S. K.; Kamykowski, D. Semianalytic moderate-resolution imaging spectrometer algorithms

for chlorophyll a and absorption with bio-optical domains based on nitrate-depletion temperatures. *J. Geophys. Res.* **1999**, *104* (C3), 5403−5421.

(67) Werdell, P. J.; Proctor, C. W.; Boss, E.; Leeuw, T.; Ouhssain, M. Underway sampling of the marine inherent optical properties on the Tara Oceans expedition as a novel resource for the ocean color satellite data production validation. *Methods in Oceanography* **2013**, *7*, 40−51.

(68) Huot, Y.; Brown, C. A.; Cullen, J. J. Retrieval of phytoplankton biomass from simultaneous inversion of reflectance, the diffuse attenuation coefficient, and sun-induced fluorescence in coastal waters. *J. Geophys. Res.* **2007**, *112*, C06013.

(69) Falkowski, P. G.; Kolber, Z. Variations in Chlorophyll Fluorescence Yields in Phytoplankton in the World Oceans. *Aust. J. Plant Physiol.* **1995**, *22*, 341−355.

(70) Merckelbach, L.; Smeed, D.; Griffiths, G. Vertical Water Velocities from Underwater Gliders. *Journal of Atmospheric and Oceanic Technology* **2010**, *27* (3), 547−563.

(71) Frajka-Williams, E.; Eriksen, C. C.; Rhines, P. B.; Harcourt, R. R. Determining Vertical Water Velocities from Seaglider. *Journal of Atmospheric and Oceanic Technology* **2011**, *28* (12), 1641−1656.

(72) Lévy, M.; Klein, P.; Treguier, A. M. Impact of sub-mesoscale physics on production and subduction of phytoplankton in an oligotrophic regime. *J. Mar. Res.* **2001**, *59* (4), 535−565.

(73) Lévy, M. The modulation of biological production by oceanic mesoscale turbulence. In *Transport and Mixing in Geophysical Flows*; Springer: Berlin Heidelberg, Germany, 2008; pp 219−261, DOI:10.1007/978-3-540-75215-8.

(74) Omand, M. M.; D'Asaro, E. A.; Lee, C. M.; Perry, M. J.; Briggs, N.; Cetinić, I.; Mahadevan, A. Eddy-driven subduction exports particulate organic carbon from the spring bloom. *Science* **2015**, *348*, 222−225.

(75) Pietri, A.; Testor, P.; Echevin, V.; Chaigneau, A.; Mortier, L.; Eldin, G.; Grados, C. Finescale vertical structure of the upwelling system off southern Peru as observed from glider data. *J. Phys. Oceanogr.* **2013**, *43*, 631−646.

(76) Webber, B. G. M.; Matthews, A. J.; Heywood, K. J.; Kaiser, J.; Schmidtko, S. Seaglider observations of equatorial Indian Ocean Rossby waves associated with the Madden-Julian Oscillation. *J. Geophys. Res. Oceans* **2014**, *119*, 3714−3731.

(77) Smyth, T. J. Penetration of UV irradiance into the global ocean. *J. Geophys. Res.* **2011**, *116*, C11020.

(78) Platt, T.; Gallegos, C. L.; Harrision, W. G. Photoinhibition of photosynthesis in natural assemblages of marine phytoplankton. *J. Mar. Res.* **1980**, *38*, 687−701.